Detailed stratigraphy and bed thickness of the Mars north and south polar layered deposits

Ajay B. S. Limaye,[1] Oded Aharonson,[1,2] and J. Taylor Perron[3]

Received 22 September 2011; revised 18 May 2012; accepted 22 May 2012; published 30 June 2012.

[1] The Mars polar layered deposits (PLD) likely hold an extensive record of recent climate during a period of high-amplitude orbit and obliquity cycles. Previous work has detected limited evidence for orbital signatures within PLD stratigraphy, but data from the High Resolution Imaging Science Experiment (HiRISE) permit renewed analysis of PLD stratigraphy at sub-meter scale. Topography derived from HiRISE images using stereogrammetry resolves beds previously detectable only as alternating light and dark bands in visible images. We utilize these data to measure the thickness of individual beds within the PLD, corrected for non-horizontal bed orientation. Stratigraphic columns and bed thickness profiles are presented for two sites within the NPLD, and show several sets of finely bedded units 1–2 m thick; isolated marker beds 3–4 m thick; and undifferentiated sections. Bed thickness measurements for three sites within the SPLD exhibit only one bed type based on albedo and morphology, and bed thicknesses have a larger mean and variance compared to measurements for the NPLD. Power spectra of brightness and slope derived along the measured stratigraphic sections confirm the regularity of NPLD fine bed thickness, and the lack of a dominant SPLD bed thickness. The regularity of fine bed thickness of the NPLD is consistent with quasiperiodic bed formation, albeit with unknown temporal period; the SPLD thickness measurements show no such regularity.

Citation: Limaye, A. B. S., O. Aharonson, and J. T. Perron (2012), Detailed stratigraphy and bed thickness of the Mars north and south polar layered deposits, *J. Geophys. Res.*, *117*, E06009, doi:10.1029/2011JE003961.

1. Introduction

[2] Atmospheric pressure on Mars fluctuates annually by thirty percent, causing significant interaction between the atmosphere and near-surface ice [*Hess et al.*, 1980]. On $>10^4$ yr timescales, Mars' high-amplitude, quasiperiodic orbital (i.e., orbit and obliquity) variations cause insolation cycles [*Laskar et al.*, 2004] that may profoundly impact atmospheric circulation and water ice stability. Models predict ice redistribution from the poles to lower latitudes at higher obliquity [*Forget et al.*, 2006; *Schorghofer*, 2007], and surface features—including midlatitude mantling deposits [*Head et al.*, 2003] and deposits reminiscent of terrestrial rock glaciers [*Head et al.*, 2005]—may reflect such orbital states. Numerous authors have proposed that the polar layered deposits (PLD) respond to orbital cycles [*Murray et al.*, 1973; *Ward*, 1973; *Toon et al.*, 1980; *Cutts and Lewis*, 1982; *Thomas et al.*, 1992], analogous to terrestrial Milankovitch periods driving glacial cycles [*Hays et al.*, 1976]. *Perron and Huybers* [2009] note that the apparent simplicity of Mars climate does not, however, guarantee translation of an orbital signal into a discernable bed sequence. Although the confidence attributed to detection of an orbital signal may depend strongly on the continuity of the stratigraphic record [*Cutts and Lewis*, 1982; *Sori et al.*, 2011], repeating patterns of bed thickness and organization would lend support to the hypothesis of orbital control.

[3] This study seeks such patterns in PLD stratigraphy with data sets that capture bed properties at the finest scale attainable from remotely sensed visible images. We address three principal questions. First, are the bed thickness characteristics of the previously measured NPLD stratigraphic column [*Fishbaugh et al.*, 2010b] found elsewhere in the NPLD? Second, what range of bed thickness exists in the south polar layered deposits (SPLD)? Third, how do spectral characteristics of the PLD relate to direct measurements of bed thickness and organization, using refined topographic data? Section 2 reviews general characteristics of the polar domes and previous work on PLD stratigraphy. Section 3 details methods used for topographic extraction and data analysis. Section 4 presents results of stratigraphic analyses at several sites within the PLD, which are compared to spectral estimates of PLD organization in section 5. We discuss the

[1]Division of Geological and Planetary Sciences, California Institute of Technology, Pasadena, California, USA.
[2]Now at Center for Planetary Sciences, Weizmann Institute of Science, Rehovot, Israel.
[3]Department of Earth, Atmospheric and Planetary Sciences, Massachusetts Institute of Technology, Cambridge, Massachusetts, USA.

Corresponding author: A. B. S. Limaye, Division of Geological and Planetary Sciences, California Institute of Technology, 1200 E. California Blvd., MC 170-25, Pasadena, CA 91125, USA. (ajay@caltech.edu)

0148-0227/12/2011JE003961

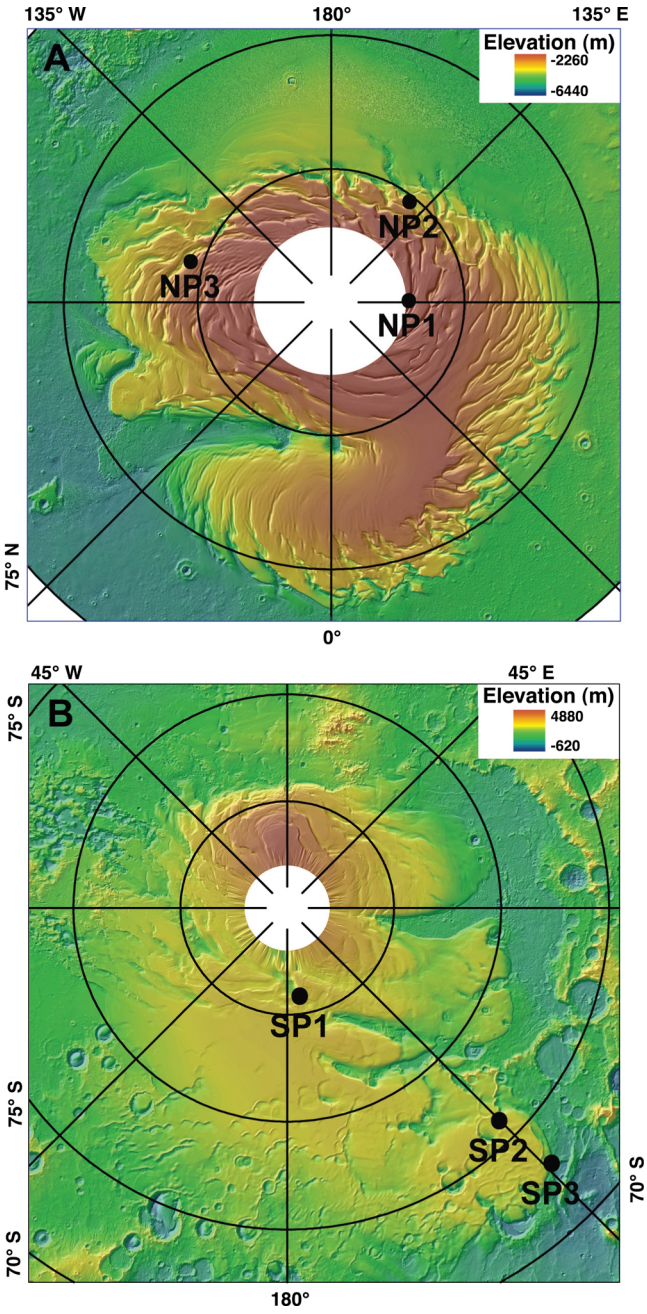

Figure 1. Locations of study sites in the polar regions of Mars. Base image is color-coded, shaded relief of Mars Orbiter Laser Altimeter (MOLA) topography. (a) NPLD sites. NP1 has been analyzed by *Fishbaugh et al.* [2010b]. Sites NP2 and NP3 are analyzed herein. (b) SPLD sites SP1, SP2, and SP3.

measurements with respect to the orbital-control hypothesis in section 6, and distill conclusions in section 7.

2. Stratigraphy of the Polar Layered Deposits

[4] Both PLD are dissected by spiral troughs, which dominate the large-scale topography of the NPLD. The SPLD extend as far equatorward as ~70°S, and form a broad plateau from 70 to 82°S and 130–230°W (Figure 1) [*Kolb and Tanaka*, 2001]. Several lines of evidence indicate that water ice comprises most of the PLD [*Mellon*, 1996; *Nye et al.*, 2000; *Bibring et al.*, 2004; *Langevin et al.*, 2005; *Zuber et al.*, 2007; *Wieczorek*, 2008; *Piqueux et al.*, 2008]. Radar data suggest a <2% and <10% dust component by mass of within the NPLD and SPLD, respectively, and also reveal that the PLD are commonly 1–2 km thick [*Picardi et al.*, 2005; *Plaut et al.*, 2007; *Phillips et al.*, 2008]. The SPLD likely harbors a buried CO_2 deposit comparable to the mass of CO_2 in the atmosphere [*Phillips et al.*, 2011]. A collection of several beds discernable in visible images may produce a single reflection in the radar data; thus detailed stratigraphic study requires visible images of PLD outcrops [*Milkovich et al.*, 2009]. Unconformities pervade both PLD [e.g., *Howard et al.*, 1982; *Tanaka*, 2005], while faulting is rare [*Byrne*, 2009]. These parallels suggest that the NPLD and SPLD share a similar composition and origin. The two units differ, however, in stratigraphic context and age.

[5] The NPLD unconformably overlie the Planum Boreum Cavi, which outcrops on the NPLD periphery and consists of beds of ice and locally cross-bedded sand [*Herkenhoff et al.*, 2007]. A meter-thick, water ice residual cap unconformably overlies the NPLD and is seasonally draped by CO_2 and water frost [*Tanaka et al.*, 2008; *Byrne*, 2009]. Few craters mark either PLD surface, particularly for the NPLD, whose surface age has been estimated at $\sim 10^5$ yr old or less [*Herkenhoff and Plaut*, 2000; *Tanaka*, 2005; *Banks et al.*, 2010]. In contrast, the population of relatively small craters implies a 10–100 Myr SPLD surface age [*Herkenhoff and Plaut*, 2000; *Koutnik et al.*, 2002]. *Pathare et al.* [2005] suggest an age of several hundred Myr to >1 Gyr due to the removal of large craters by viscous relaxation. The SPLD base is roughly 6 km higher than that of the NPLD, and overlies Hesperian and Noachian surfaces, including the Dorsa Argentea Formation [*Tanaka and Scott*, 1987]. The SPLD are covered in places by an annually persistent CO_2 ice cap of a few meters thickness, and seasonal frosts of CO_2 and occasionally water [*Byrne*, 2009].

[6] Several studies have used image analysis to construct conceptual models of large-scale SPLD accumulation. *Byrne and Ivanov* [2004] used the orientation of a widespread and prominent topographic bench to infer a domical structure. *Milkovich and Plaut* [2008] interpret the SPLD to consist of three distinct units with different areal extents, which include (from stratigraphically highest to lowest) the Bench-Forming Layer sequence, a distinct layered sequence termed the Promethei Lingula Layer sequence, and a buried unit inferred from radar observations [*Plaut et al.*, 2007].

[7] A number of theoretical studies have investigated connections between Mars climate and the growth of PLD stratigraphy. *Toon et al.* [1980], *Cutts and Lewis* [1982], *Jakosky et al.* [1993] and *Jakosky et al.* [1995] approached polar deposit evolution through one-dimensional energy balance models. More recently, *Levrard et al.* [2007] simulated PLD growth with meridional water vapor exchange calculated from a global circulation model, and parameterized dust activity; discrete beds formed with the aid of a sublimation dust lag effect. Models that involve dust can generally produce PLD beds in response to insolation variations, but have not been designed to reproduce the number, thickness, and albedo characteristics of beds at a particular location. Distinct beds could form in several ways, including

through changes in the ice to dust ratio, variations in ice or dust grain size, or depositional hiatuses [*Cutts and Lewis*, 1982; *Levrard et al.*, 2007]. Quasiperiodic forcing of ice deposition could result in ordering or clustering of bed thickness values. Noachian bedrock outcrops in Arabia Terra exhibit such periodicity: several outcrops possess narrowly distributed bed thicknesses, including a location in Becquerel crater where beds are topographically grouped in bundles [*Lewis et al.*, 2008]. In addition to recording orbital forcing, trends in PLD bed thickness with depth could hold information on water or dust supply in different climate states and the influences compaction and flow. For example, compaction should cause beds to thin with depth in a stratigraphic column due to increasing overburden.

[8] Several previous studies have sought to identify an orbital signature in PLD stratigraphy, and image data acquired in the last decade has revealed the polar landscape in increasing detail. *Fenton and Herkenhoff* [2000] used photoclinometry and point-measurements of elevation from stereogrammetry using *Viking* images, as well as Mars Orbiter Laser Altimeter (MOLA) data, to identify beds between 10 and 100 m thickness in a single NPLD trough. Several investigators analyzed brightness profiles of the upper few hundred meters of the NPLD using higher-resolution Mars Observer Camera (MOC) images and MOLA topography, with the aim of capturing periodicity in the stratigraphic record. The interior troughs of Planum Boreum only expose this upper section of the NPLD, while larger sections are exposed closer to the perimeter [*Byrne*, 2009]. *Laskar et al.* [2002] found a spectral peak at ~26 m in a MOC image, and tuned the time represented by the image brightness profile to the modeled insolation history in order to estimate ice accumulation rates. *Milkovich and Head* [2005], *Milkovich et al.* [2008] and *Perron and Huybers* [2009] assessed periodicity using the same data sets, but for a much larger suite of sites. Power spectra of NPLD brightness derived by *Milkovich and Head* [2005] and *Milkovich et al.* [2008] show peaks from 23 to 35 m wavelength in several images, but *Perron and Huybers* [2009] found only a ~1.6 m wavelength signal consistently exceeds the red noise background common to PLD brightness spectra.

[9] Correlation studies have also benefited from increased image and topography resolution. *Fishbaugh and Hvidberg* [2006] used MOC images and MOLA topography to correlate two bed sequences within the upper 500 m of NPLD stratigraphy, and inferred that relative net ice accumulation rates varied by as much as a factor of two within each sequence. *Kolb and Tanaka* [2001], *Malin and Edgett* [2001], and *Milkovich and Head* [2005] also report NPLD bed correlations across large distances. *Kolb and Tanaka* [2006] identified beds that were continuous over >150 km along canyon walls in Australe Sulci, while *Milkovich and Plaut* [2008] discontinuously correlated individual beds and bed sequences across the entire SPLD and found that individual sequence thicknesses varied by up to a factor of four over several hundred kilometers.

[10] Relating the various unconformities within the SPLD to each other and the surrounding stratigraphy represents a prominent need for establishing stratigraphic relationships. SPLD unconformities range in elevation from 1500 to 3200 m, but have resisted correlation due to limited bed exposure stratigraphically above and below [*Milkovich and Plaut*, 2008]. In their study of the Promethei Lingula region, *Kolb and Tanaka* [2006] used mapping of bed orientations and unconformities to also infer three primary PLD accumulation periods separated by major hiatuses. Although at least one regional stratigraphic mapping study [*Kolb and Tanaka*, 2006] has established a framework for relating unconformities near one of our study sites (SP3), the intervening distance is too large to confidently correlate unconformities without extensive image analysis and is beyond the scope of this study.

[11] Where High Resolution Imaging Science Experiment (HiRISE) [*McEwen et al.*, 2007] image pairs and MOLA altimetry data are available (below 87° latitude), stereogrammetry-derived digital elevation models (DEMs) have superseded the MOLA elevation data set central to many of the aforementioned studies, and permit direct bed thickness measurements. A 400 m section of the upper NPLD [*Fishbaugh et al.*, 2010b] shows undifferentiated sections, groups of fine beds (thicknesses 1–2 m) and dark, topographically prominent marker beds, so-named because similar beds have been observed to correlate over large distances [*Malin and Edgett*, 2001; *Fishbaugh et al.*, 2010a]. Where appropriate we adopt the same bed classification, with the caveat that we do not evaluate whether the marker beds discussed herein are expressed elsewhere in the NPLD stratigraphy.

[12] Beds within the SPLD are more uniform in albedo; the majority of the exposed stratigraphy has been mapped as a single layered unit, termed the Planum Australe 1 unit [*Tanaka and Kolb*, 2005]. The main correlated sequence [*Milkovich and Plaut*, 2008], the Promethei Lingula Layer sequence (after its type locality), also belongs to this unit. A relatively thin, overlying horizon has been distinguished by its pitted and knobby texture as the Planum Australe 2 unit [*Tanaka and Kolb*, 2005] and as the Bench-Forming Layer sequence [*Milkovich and Plaut*, 2008], after the horizon identified by *Byrne and Ivanov* [2004]. The work presented herein is focused on the Planum Australe 1 unit. Because beds within this unit lack textural or albedo differences with which to distinguish bed types, no facies-based stratigraphic columns are generated for the SPLD sites described herein. In contrast, the variability between the marker beds and fine bed sets in the NPLD enables mapping boundaries between these bed types. As noted by *Byrne* [2009], SPLD beds commonly form topographic benches, while in profile NPLD beds protrude less distinctly from trough slopes. As in the NPLD, some SPLD bed boundaries are gradational due to a combination of erosive and depositional processes [see *Fishbaugh et al.*, 2010a].

[13] SPLD bed thickness and stratigraphic periodicity has garnered limited attention in previous work. *Herkenhoff and Kirk* [2001] derived bed thicknesses of ~10 m within the SPLD using MOC image photoclinometry, and suggested the presence of thinner beds. *Byrne and Ivanov* [2004] measured beds in Australe Mensa at several meters thick, while *Milkovich and Plaut* [2008] estimated bed thicknesses ranging from ~5–40 m on the basis of ~17 m/pixel Thermal Emission Imaging System (THEMIS) images and MOLA topography. *Milkovich et al.* [2008] found a principal wavelength of 35 m in MOC image brightness at one SPLD location. Mars' chaotic obliquity evolution limits inference of insolation prior to 10–20 Ma [*Laskar et al.*, 2004], which

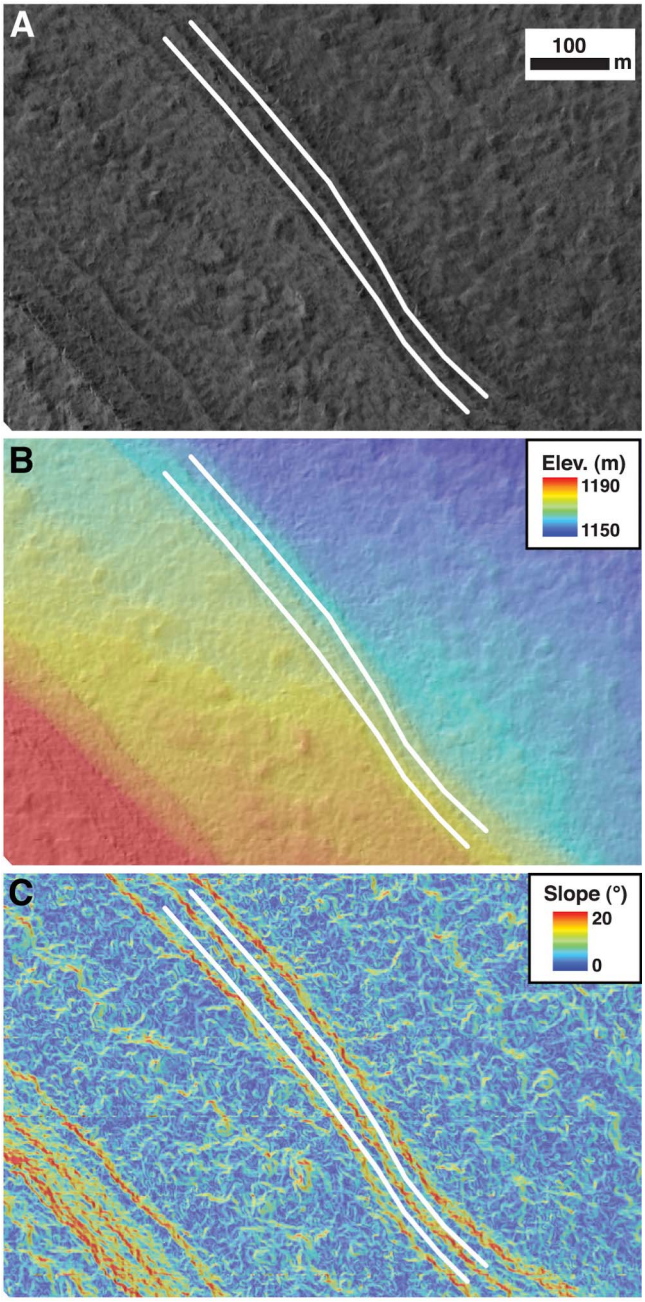

Figure 2. Illustration of bed thickness measurement technique, using a single bed at site SP3. Pixel values are extracted along white profile lines, which delineate bed ledge surfaces. (a) Orthophoto produced using HiRISE image ESP_013277_1070. (b) Digital elevation model, which shows that right profile samples the lower bounding surface, and left profile samples the upper bounding surface. (c) Slope map. Bed risers possess relatively high slopes (red-orange), while bed ledges possess relatively lower slopes (blue-green).

likely precludes direct comparison of modeled insolation to SPLD stratigraphic columns. A periodic component to SPLD stratigraphy nonetheless remains possible.

[14] This work presents stratigraphic columns and bed thickness distributions at two sites within the NPLD, as well as the first three bed thickness distributions within the SPLD at the scale of HiRISE image data. Because the presence of undifferentiated sections limits the continuity of direct bed thickness measurements, and for comparison to previous analyses, we also perform spectral analysis of slope and image brightness to characterize the dominant spatial scales of bed organization.

3. Bed Thickness Measurement Methods

3.1. Bed Identification

[15] With existing data sets, beds are definable using image brightness, meter-scale topography, or a combination of the two. Though previous studies of NPLD bed thickness have mostly utilized image brightness, this property has been demonstrated to vary with lighting conditions, surface roughness, and the presence of frost or dust veneers [*Fishbaugh et al.*, 2010a]. As an alternative method of bed delineation, high-resolution DEMs allow bed definition by breaks in slope in shaded relief maps, but the topographic irregularity from mantling deposits and erosive processes (including eolian modification, slumping, and sublimation pitting) is similar in magnitude to the stratigraphic thickness of the finest visible beds in the NPLD [*Fishbaugh et al.*, 2010a]. Thus the topography does not consistently reveal distinct bed surfaces. In practice, light and dark bands observed in images are laterally continuous and commonly do coincide with slope transitions in the co-registered DEM. Consequently, in this study, where beds are apparent from image brightness but indistinct in shaded relief, we determine the brightness corresponding to the ledge (sub-horizontal surface) and slope of each bed as long as a locally high slope (in the DEM) occurs between the bright and dark bands (in the orthophoto). Where the beds are distinct in shaded relief, the shaded relief map is used to delineate bed ledges. The difference of successive ledges is taken as the apparent bed thickness (Figure 2). We assume similar controls on image brightness of SPLD surfaces [*Milkovich and Plaut*, 2008] as has been investigated in the NPLD [*Fishbaugh et al.*, 2010a], and that the topographic criteria used to identify bed ledges and slopes are equally applicable to beds in both PLD.

3.2. Image Processing and DEM Extraction

[16] DEMs are generated with methods similar to previous studies [*Kirk et al.*, 2008; *Lewis et al.*, 2008; *Fishbaugh et al.*, 2010a]. HiRISE image resolution is typically 25 cm/pixel. Each pair of images undergoes radiometric calibration, correction for detector orientation and optical distortions, and mosaicking using the U.S. Geological Survey's Integrated Software for Imagers and Spectrometers 3. Topography is derived from the images using BAE Systems' SOCET SET following methods similar to *Kirk et al.* [2008] and *Lewis et al.* [2008]. The elevations of surface points common to each image are controlled using individual MOLA retrievals and gridded data. All DEMs possess residuals—the discrepancy between feature locations and their predicted locations based on the sensor model—with a maximum root-mean square of 0.70 pixel. Initial DEM quality control entails plotting contours of the extracted topography over the source images to check alignment with the surface. Finally, one HiRISE image is ortho-rectified with respect to the DEM to

Table 1. Summary of Bed Thickness and Orientation Data[a]

Site	Location	Figures	Bed Thicknesses Measured	Mean Bed Thickness and Std. Dev. (m)	Mean Dip Azimuth and Error (°)	Mean Dip Magnitude and Error (°)
NP2	85.1°N, 143.1°E	3, 5a, 9a, 9b, S1	12	1.7 (0.3)	79.6 (0.7)	0.6 (0.1)
NP3	84.4°N, 253.1°E	4, 5b, 8, 9c, 9d, S2	30	1.8 (0.6)	40.5 (0.3)	0.8 (0.1)
SP1	86.1°S, 172.0°E	6a, S3	18	5.7 (3.1)	73.2 (1.3)	2.7 (0.3)
SP2	76.2°S, 134.5°E	6b, S4	23	1.8–46.3 (range)	14.5–354.5 (range)	0.2–1.3 (range)
SP3	73.1°S, 133.5°E	2, 7, S5	25	12.2 (7.8)	36.9 (1.6) 226 (0.4) 4.0 (0.5)	4.7 (0.5) 3.8 (0.4) 2.5 (0.3)

[a]Orientation measurements for site SP3 correspond to lower, middle, and upper sections, respectively.

correct the image for optical distortion. High-frequency vibrations unresolved by spacecraft orientation kernels cause decimeter-scale elevation discontinuities at CCD boundaries, and failure of the pixel correlation algorithm also contributes artifacts in limited regions, which are clearly visible in the shaded relief and avoided for analysis.

3.3. Correction for Non-Horizontal Bed Orientation

[17] For each site, the orthophoto, DEM, and shaded relief map are examined concurrently (Figure 2). An equidistant cylindrical projection centered on the latitude of the image is used at all sites. We measure bed orientation by fitting a plane to the bed ledge. Using the orthophoto and shaded relief map, the orientation of each discernable bed is measured by tracing a profile along the bed ledge, interpolating the DEM for elevation along the profile, and determining the best fit plane using multiple linear regression. We fit the equation of a plane:

$$z = ax + by + c \tag{1}$$

The dip azimuth (θ) and magnitude (ϕ) are determined from the regression coefficients using:

$$\tan(\theta + \pi) = b/a \tag{2a}$$

$$\tan\phi = \left(a^2 + b^2\right)^{1/2} \tag{2b}$$

A bed ledge must have appreciable planform curvature or width to allow a well-constrained plane fit, so some beds do not permit meaningful orientation measurements. Therefore in moving up-section, we assume that a group of adjacent beds possesses a consistent orientation until a measurement higher in the stratigraphic section suggests a change in orientation. Any regression solutions for which the uncertainty in the fitted plane's pole orientation exceeds 1° are disregarded. Orientation information enables projecting the elevation of each bed ledge to a common stratigraphic reference frame. A dip correction yields the stratigraphic distance between bed ledges (i.e., derived true bed thickness).

[18] Shallow topographic slopes enhance bed exposure; thus the effective stratigraphic resolution is generally finer than the typical 1 m horizontal resolution of the DEM and orthophoto. Consequently, any beds that escape detection would have to be much finer than a few decimeters in thickness [*Herkenhoff et al.*, 2007; *Lewis et al.*, 2008]. Topography has been modeled at five sites (Figures 1 and S1–S5), based on the availability of HiRISE observations suitable for stereogrammetry, and the quality of bed exposure.[1] Site-specific bed thicknesses and orientations are shown in Table 1. Stratigraphic sections are oriented to sample topographically distinct beds and to maximize section height.

3.4. Bed Thickness Measurement Error

[19] We consider error in bed thickness measurements from three sources: imprecise bed identification, uncertainty in bed orientation, and errors in the DEM (Table 2). To estimate the error in bed ledge identification, an independent investigator delineated bed ledges in previously measured locations at two sites (sites NP2 and SP1), which contained 30 beds with measured thicknesses from 1 to 12 m (Figure S6). Bed thickness measurements by different investigators using the plane differencing technique show no consistent trend in measurement error as a function of stratigraphic position. Although most beds less than 5 m thick at site SP1 possess higher relative error than those at site NP2, this trend is inconsistent and may not be significant given the limited number of SP1 beds in that thickness scale range. We also conducted point measurements of true (dip-corrected) bed thickness over more than a kilometer laterally at these sites to characterize lateral bed thickness variability at the scale of stratigraphic horizon averaging.

[1]Auxiliary materials are available with the HTML. doi:10.1029/2011JE003961.

Table 2. Contributions to Bed Thickness Measurement Error at Each Site

Site	DEM Vertical Precision (m)	Bed Profile Standard Error From DEM (100 Meas.) (m)	Bed Thickness Standard Error From DEM (m)	Median Relative Error Due to Bed Orientation (%)	Estimated Relative Error in Bed Ledge Identification (%)
NP2	0.5	0.05	0.07	0.2	10
NP3	0.4	0.04	0.06	0.1	10
SP1	0.7	0.07	0.09	0.7	10
SP2	0.4	0.04	0.05	0.3	10
SP3	0.5	0.05	0.08	Sect. 1, 1.0 Sect. 2, 0.2 Sect. 3, 1.0	10

Both methods suggest a median relative uncertainty in bed thickness of about 10% owing to differences in where a bed ledge is sampled.

[20] Surface roughness and bed ledge deviation from planarity contribute to uncertainty in a fitted plane's orientation. We estimate the uncertainty in bed thickness arising from the planar fit using a Monte Carlo technique. For each group of beds assumed to share the same orientation, bed thickness is calculated using the subset of well-constrained orientation measurements. The average of the planar regression coefficients and their 1-σ confidence intervals are used to generate a population of 1000 normally distributed values of dip azimuth and magnitude (mean and standard deviation listed in Table 1). For each set of orientation angles, the bed thickness is calculated from the difference of stratigraphic heights (c in equation (1)) for each ledge. We calculate the error as the standard deviation in thickness for each individual bed, as measured from the calculated population of orientations for the suite of beds. Our measurements show the relative magnitude of this error source to be $\leq$1% of bed thickness for all measured beds (Table 2).

[21] An additional contribution to error in stratigraphic height results from errors in the DEM. The theoretical DEM vertical precision is a function of spacecraft position, image resolution, and pixel correlation error [see *Kirk et al.*, 2008; *Fishbaugh et al.*, 2010a; *Okubo*, 2010], and is listed in Table 2 for each site. Although vertical precision at the study sites ranges from 0.4 to 0.9 m, we reduce the standard error by averaging stratigraphic height determined from equation (1) over at least 100 locations along a bed ledge, which reduces the error in ledge stratigraphic height to by a factor of at least 10. Since bed thickness is determined using the difference of the upper and lower bed boundaries, the absolute error in thickness of each bed is determined using the following equation

$$E_{t,i} = \sqrt{e_{a,UL}^2 + e_{a,LL}^2 + \left(e_{r,s}t_i\right)^2 + \left(e_{r,o}t_i\right)^2}$$

where $E_{t,i}$ is the absolute error in thickness in bed i with thickness t_i, $e_{a,UL}$ is the absolute in error upper bed ledge stratigraphic height, $e_{a,LL}$ is the absolute error in lower bed ledge stratigraphic height, $e_{r,s}$ is the relative error due to subjectivity in bed delineation, and $e_{r,o}$ is the relative error due to uncertainty in bed orientation.

4. Stratigraphy and Bed Thickness Within the PLD

4.1. Sites NP2 and NP3

4.1.1. Site NP2

[22] Site NP2 (Figure 1 and S1) occupies a trough wall with a rounded exposure of NPLD and relief in excess of 1 km. The exposed section lies within the Planum Boreum 1 unit [*Tanaka et al.*, 2008], which comprises most of the NPLD, and is near its periphery. Bright frost, perhaps seasonal, obscures the highest beds at the site. An angular unconformity is present, and is extrapolated to a paraconformity within the measured section (Figure 3); this may represent a period of erosion.

[23] Three distinct sets of fine beds exist within the measured stratigraphic column. Structural measurements taken from the middle and upper fine-bedded sections indicate a consistent dip with an average magnitude of 0.6°. The lowermost thin bed set begins beneath the starting point of the column, and possesses a stratigraphic thickness greater than 45 m. Some beds of the lower thin bed set exhibit local slumping, but most remain intact; however, contacts between fine beds at the top of the set are gradational. Immediately above the lower fine bed set is a dark, topographically prominent marker bed, with some surface erosion. Undifferentiated sections bracket the middle fine bed set, which has a thickness of ~25 m. The top of the middle undifferentiated section includes partially obscured fine beds. The top thin bed set proceeds upward for ~10 m before terminating in another undifferentiated section. As observed by *Fishbaugh et al.* [2010b] for site NP1, the bed types at site NP2 are sets of fine beds that alternate with thicker, darker marker beds, and undifferentiated sections. In places the undifferentiated sections show traces of smoothed fine beds [*Fishbaugh et al.*, 2010a], while some sections bereft of apparent bedding might have been deposited as massive units. Bed thicknesses were directly measured where attainable, and compared to relative stratigraphic height within the measured section (Figure 5a). All of the beds measured belong to fine bed sets, because of ambiguous marker bed boundaries. The directly measured beds all possess thicknesses between 1 and 2 m, and are similar in thickness to the fine beds measured at site NP1 [*Fishbaugh et al.*, 2010b]. The uppermost beds thin with depth, while the lowermost beds thicken with depth; however neither group contains enough beds for these trends to be statistically significant.

4.1.2. Site NP3

[24] Site NP3 (Figure 1 and S2) occupies a topographically complex region between two local highs. Thickness measurements and bed types were noted along the transect shown in Figure S2. Structure measurements from beds in the lower and middle part of the transect indicate a consistent dip with an average magnitude of 0.7°. As with sites NP1 and NP2, site NP3 lies within the Planum Boreum 1 unit [*Tanaka et al.*, 2008]; the distance from site NP3 to the NPLD periphery is intermediate between the equivalent distances for NP1 and NP2 (Figure 1). Small amounts of frost highlight particular beds, but other mantling deposits partially drape bed exposures. Some unit contacts are gradational, but many of the fine beds remain topographically well defined.

[25] The stratigraphic column (Figure 4) shows that four sets of fine beds are present, the lower two of which are each less than 10 m thick. The lower two fine bed sets are separated by an undifferentiated unit, which nonetheless contains a few faint, continuous horizons that appear to represent mantled fine beds. The upper two sets of fine beds possess similar collective thicknesses (~62 m for the lower, ~58 m for the higher). Except for the bottom fine bed set, all fine bed sets are overlain by an undifferentiated unit and then a marker bed above. Notably, the fine beds again cluster between 1 and 2 m thickness (Figure 5b), whereas the marker beds form a distinct thickness population with thickness 3.0–3.6 m. Fine bed thickness shows no trend with depth in the section. Measured bed thicknesses are comparable in magnitude to those at sites NP1 and NP2. The separation distances observed between marker beds (~74 m,

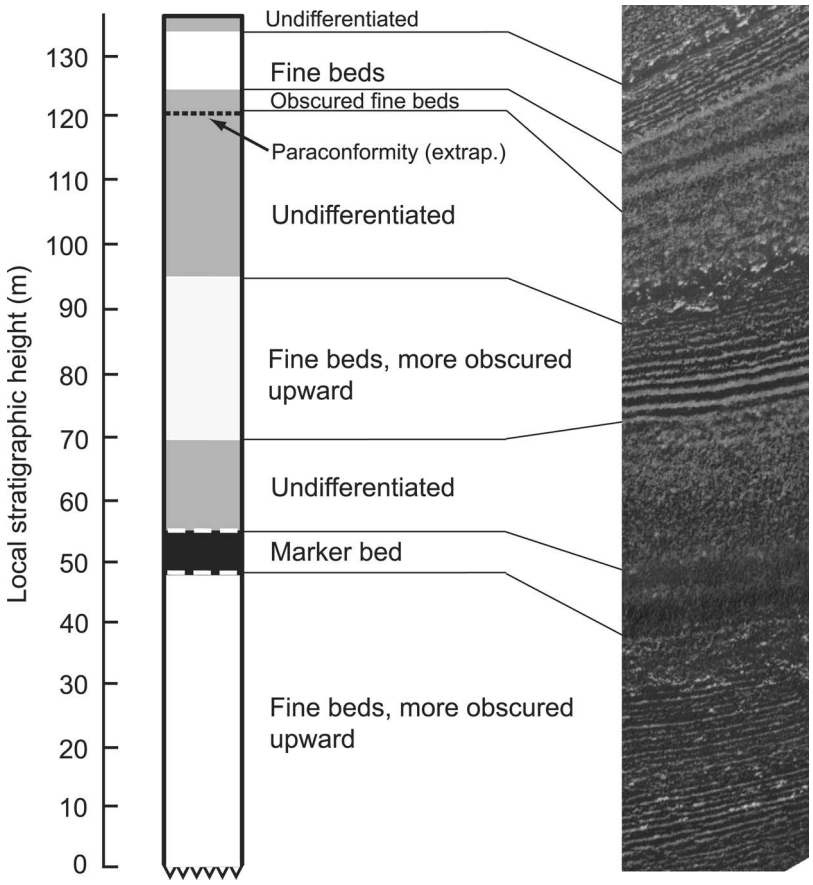

Figure 3. Stratigraphic section of site NP2. Fine bed sequences are shaded white, undifferentiated units gray, and marker beds black. At right, the corresponding portion of orthorectified image PSP_010014_2650. Black lines demarcate unit contacts. White dashed line demarcates tentative marker bed contact. Sawtooth lower boundary on stratigraphic column indicates that fine beds continue below the lower edge of the image. Black dashed line shows extrapolated location of paraconformity (see Figure S1). Maximum horizontal scale of image is approximately 500 m.

~67 m) are much greater than the 24–36 m separation distance which would correspond to the peak in spectral power at that wavelength noted by *Milkovich and Head* [2005] in many sections of the NPLD. *Fishbaugh et al.* [2010b] note that the 24–36 m separation distance corresponds to only half of the marker beds at site NP1.

4.2. Sites SP1, SP2, and SP3

4.2.1. Site SP1

[26] Site SP1 (Figure 1 and S3) occupies a trough in the interior of the SPLD [*Tanaka and Scott*, 1987]. The highest surface has a morphology similar to the broad, pitted surfaces of the Bench-Forming Layers (BFL) [*Byrne and Ivanov*, 2004] and exists within their mapped planview extent [*Milkovich and Plaut*, 2008], but all measurements at this site are made below the potential BFL horizon. The site contains over 20 beds exposed along the measured transect, and no angular unconformities are apparent. Structure measurements indicate a mean dip of 2.7°. We extracted measurements from two sets of locations along the transect, which are separated by a section where bedding is present but indistinct. The bed thickness distribution (Figure 6a) shows a larger spread in bed thickness than observed for the NPLD sites, and a larger mean thickness. Bed thickness decreases non-monotonically with depth.

4.2.2. Site SP2

[27] Site SP2 (Figure 1 and S4) exhibits an outcrop with concentrically exposed beds, in the Ultimi Lobe near the margin of the SPLD [*Tanaka and Scott*, 1987]. This region, which includes site SP3, is the principal zone of brittle deformation within the SPLD [*Murray et al.*, 2001; *Kolb and Tanaka*, 2001; *Milkovich and Plaut*, 2008]; however no faults are observed at either of the study sites. Based on their planview location, the beds at these two sites belong exclusively to the PLL interpreted by *Milkovich and Plaut* [2008]. At site SP2, nine structure measurements show dip magnitudes ≤1.3° with widely varying azimuths; the well-constrained and small dip magnitude leads to a relatively small uncertainty in bed thickness measurements. The scatter in bed orientations results, at least in part, from the hummocky bed surfaces from which they are derived. A prominent angular unconformity intersects the study section near the transect area and likely transitions to a paraconformity within the measured section (Figure S4). The thickness measurements show a similar spread in bed thickness compared to site SP1, but also include several beds with thickness greater than 20 m. As at site SP1,

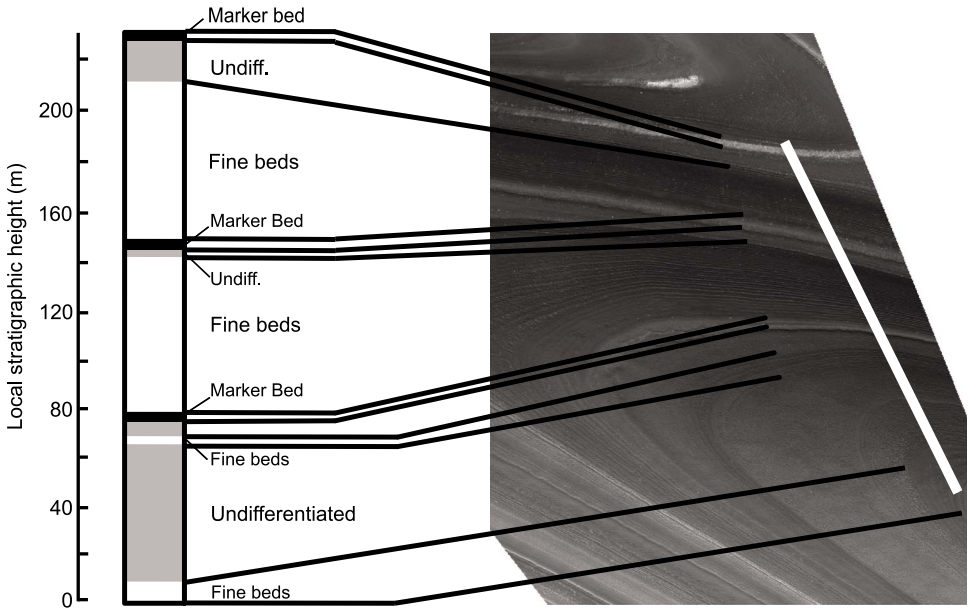

Figure 4. Stratigraphic section of site NP3. Column shading matches that in Figure 3. At right, the corresponding portion of orthorectified image PSP_010004_2650. Black lines demarcate contacts. White line indicates measurement transect. Maximum distance across image is approximately 5.5 km.

bed thickness decreases non-monotonically with depth (Figure 6b); given the caveat of a small sample size, regression analysis indicates a significant association between depth and thickness at both sites SP1 ($n = 18$, $p = 0.02$) and SP2 ($n = 23$, $p = 0.04$).

4.2.3. Site SP3

[28] Site SP3 (Figure 1 and S5) also lies near the SPLD margin [*Tanaka and Scott*, 1987]. The site possesses substantial relief (>500 m) and generally well-exposed beds. Bed orientation measurements reveal structure not immediately obvious based on the image alone. The measured section possesses three groups of beds with different orientations. While dip magnitude ranges from 2.2 to 5.2° within the transect, dip direction varies markedly between, but not within, the three sections (Table 1). Although bed truncations that would separate these sections are difficult to isolate in the image, we tentatively interpret each of these sections to be separated by angular unconformities based on the three distinct structural zones. We also note two more prominent angular unconformities, including one near the upper portion of the middle section (Figure S5). The lower and upper sections show measured bed thicknesses ranging from 1 to 5 m, while the upper section ranges in bed thickness from roughly 5 to 27 m (Figure 7). Bed thickness decreases with depth in the middle section, but increases with depth in the lower 50 m. No robust trend in thickness is observed leading up to either unconformity.

5. Spectral Estimates of PLD Periodicity

5.1. Methods

[29] In contrast to the direct measurements of bed thickness and the stratigraphic succession of bed types presented in the previous section, spectral analysis can be used to objectively infer the characteristic spatial scales associated with a stratigraphic section as a whole and can reveal scales of organization beyond the thickness of individual beds [e.g., *Lewis et al.*, 2008]. We have performed spectral analysis of image brightness and slope profiles from each of the five study sites, using the multitaper method [*Thomson*, 1982], which limits leakage of spectral power into sideband frequencies. Brightness and slope are retrieved from the locations of the measured stratigraphic section at each site (Figures S1–S5). Because multiple factors can influence surface brightness, we concurrently analyze slope derived solely from the DEM in order to determine if slope and brightness yield consistent results.

[30] Climate time series commonly show enhanced power at low frequencies [*Mann and Lees*, 1996], a behavior mirrored by power spectra of PLD image brightness [*Perron and Huybers*, 2009]. Consequently, we evaluate the significance of spectral peaks with respect to a modeled red noise background, using the robust estimation technique of *Mann and Lees* [1996]. Red noise is modeled as a first-order autoregressive process

$$r_n = \rho r_{n-1} + w_n \tag{3}$$

where r_n is red noise, ρ is the lag-one autocorrelation coefficient, and w_n is Gaussian white noise.

[31] The algorithm generates a modeled red noise spectrum from input data by (1) identifying and removing narrow-band peaks from the multitaper power spectrum; (2) smoothing the power spectrum by replacing the power estimate at each frequency with the median of a window centered on that frequency; and (3) optimizing a red noise model, in the least squares sense, for the remaining spectrum, for the lag-one autocorrelation coefficient and the average value of the spectrum. Confidence levels are computed assuming a χ^2-distribution of spectral power with six

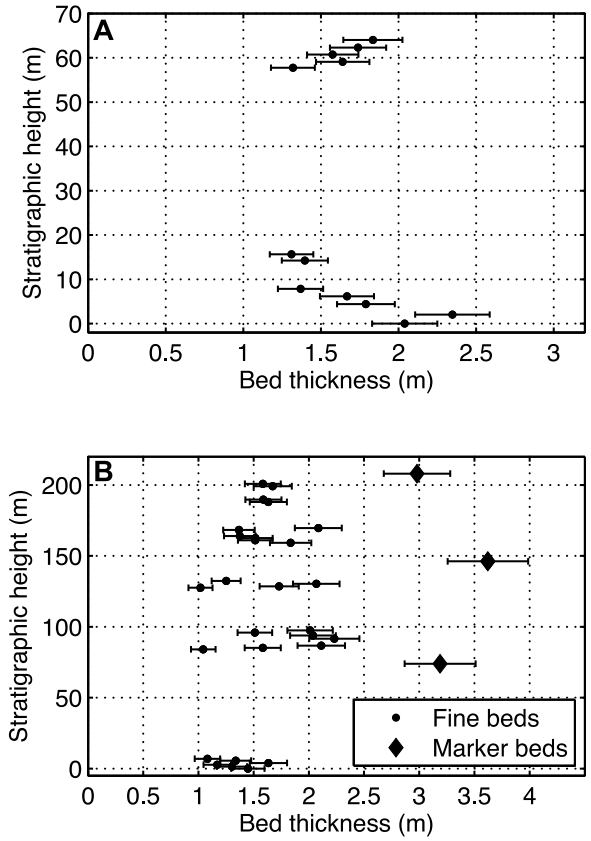

Figure 5. Relative stratigraphic height versus bed thickness for NPLD stratigraphic sections. (a) Site NP2. The number of thickness measurements represents the number of directly measured beds; many other beds are present, but are more poorly exposed or more highly eroded. (b) Site NP3. The three beds with thickness greater than 2 m are all marker beds; the rest belong to fine bed units.

degrees of freedom, where the degrees of freedom are proportional to the number of data tapers [*Mann and Lees*, 1996]. The brightness and slope data are corrected for topography and bed orientation, and sampled at 0.1 m^{-1} frequency in the local stratigraphic reference frame. A linear trend is removed from the data and the derived spectra utilize three Slepian data tapers and a smoothing interval of 0.2 m^{-1}; derived spectra and confidence levels vary slightly using a reasonable range of these parameters, but remain qualitatively similar.

5.2. NPLD Spectra

[32] Power spectra from site NP3 show several peaks exceeding the 99% confidence level in both image brightness and slope (Figure 8). Some peaks fall within the 1-σ range of measured bed thickness at the site, while others occupy shorter wavelengths. Power spectra at site NP2 show similar characteristics, with the brightness spectrum showing one peak at slightly longer wavelength than the 1-σ range of bed thickness at that site. When the sampling is restricted to portions of the stratigraphy which contain only fine beds, the most power is associated with beds that fall within the 1-σ range of measured bed thickness at both sites NP2 and NP3, and the spectral peaks are significant at the 99% confidence level (Figure 9). This directly demonstrates the correspondence between a significant peak in spectral power and a direct thickness measurement in the PLD, a relationship suggested in previous studies [*Perron and Huybers*, 2009; *Fishbaugh et al.*, 2010b]. Notably, the peak in spectral power associated with the repeating thickness of fine beds is much less conspicuous in a typical stratigraphic section that contains fine beds, marker beds, and undifferentiated sections. No repeating scale of bed organization greater than the 1-σ range of measured bed thicknesses is observed.

5.3. SPLD Spectra

[33] Power spectra of slope and brightness in the SPLD reflect the broad range of measured bed thicknesses. Figure 10 shows a representative power spectrum of slope for the measured stratigraphic section at site SP1. Only one peak exceeds the 99% confidence level. The direct bed thickness measurements do not show clustering around this peak, but rather span a range of greater thicknesses. This may result from difficulty in identifying bed boundaries in limited portions of the section. Power spectra of slope and brightness at sites SP2 and SP3 (middle section) likewise show no dominant spectral peak; several peaks exceed the

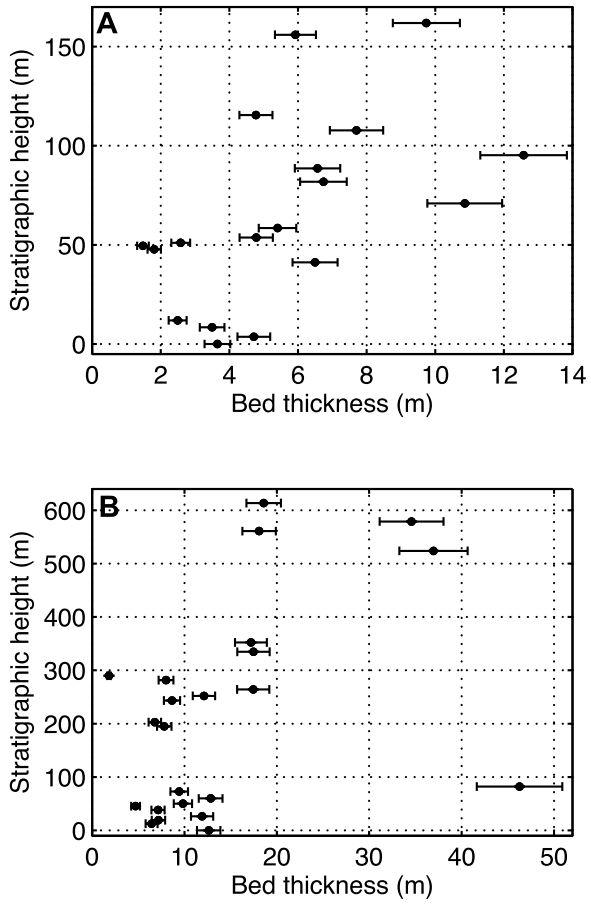

Figure 6. Relative stratigraphic height versus bed thickness for (a) site SP1, and (b) site SP2.

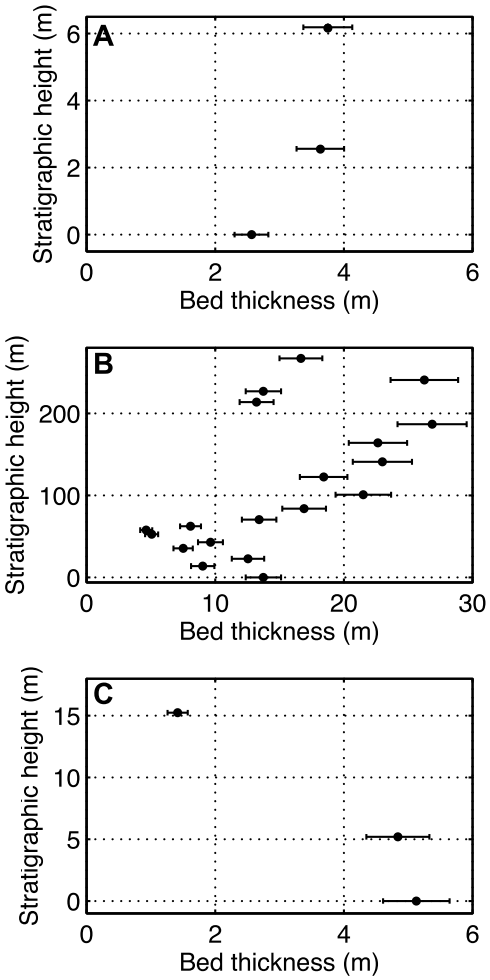

Figure 7. Relative stratigraphic height versus bed thickness for site SP3. (a) Upper section; (b) middle section; (c) lower section. Sections are grouped by bed orientation.

99% confidence level, but show little correspondence to the measured 1-σ range of bed thicknesses at those sites. The SPLD power spectra confirm direct thickness measurements, which imply that the SPLD sites lack a repeating bed thickness.

[34] Several derived power spectra contain peaks at long wavelengths from 30 to 250 m. These features could arise from large-scale changes in composition or surficial modification. However, the stratigraphic length-scales of the measured transects, at a few hundred meters, are too short to assert the periodicity of long-wavelength features. Therefore, although long-wavelength features do contribute to the spectral signatures of slope and brightness, they do not represent repeating stratigraphic features at the scales of probed by this study. In the specific context of identifying periodic signals in the stratigraphy, it is important to look for signals at similar wavelengths in different records because even a random signal will occasionally exceed the background. However, long-wavelength peaks are not observed to occur at the same wavelengths in either slope or brightness at any of the study sites, and do not correlate between sites. In contrast, the spectral signal of fine beds is observed in slope and brightness records at both NPLD sites, and the wavelength of the fine bed signal is much shorter than all stratigraphic record lengths.

6. Discussion

[35] The stratigraphic columns and bed thickness measurements presented herein and in *Fishbaugh et al.* [2010b] suggest that beds of 1–2 m thickness are common within the Planum Boreum 1 unit of the NPLD. Taken together, the thickness of fine beds at sites NP2 and NP3 is consistent with a normal distribution at a 95% confidence level via the Kolmogorov-Smirnov test, comparing the observed distribution (n = 39) to a theoretical one with the same mean and variance [*Lilliefors*, 1967]. While fine bed thickness is tightly distributed, the fine bed package thickness varies considerably. The moderate side slopes of the PLD troughs strongly enhance stratigraphic resolution to a typical sample interval of ~10 cm, in principle allowing our analysis to detect periodic signals with a stratigraphic wavelength as short as ~20 cm. The reduced spectral power at these short wavelengths implies that any beds thinner than the thinnest measured here—1.0 m for the NPLD, 1.4 m for the SPLD—must be several times thinner [*Herkenhoff et al.*, 2007].

[36] Marker bed thickness, fine bed set thickness, and the separation distance between marker beds are less consistent than fine bed thickness, also in agreement with the findings of *Fishbaugh et al.* [2010b] for site NP1. Wavelet analysis of MOC images of the upper NPLD commonly indicates thinning with depth [*Perron and Huybers*, 2009], and *Fishbaugh et al.* [2010b] suggest that beds at site NP1 show a weak marker bed thinning trend with depth. Among NPLD bed thickness measurements presented here, the only observed trend is a weak thinning with depth of the fine beds at site NP3. All of the SPLD sites show non-monotonically decreasing bed thickness with depth. The large magnitude of the thickness difference (a factor of several) between beds near the top of these sections versus beds near the bottom, as well as the trend's reversal in the middle section of site SP3, argues against compaction serving as the dominant thinning mechanism. Rather, we speculate that the trends in thickness in the SPLD sections result from changes in deposition rates or bed preservation potential.

[37] The beds of 1–2 m have been confirmed to correspond to the rise in spectral power above a modeled red noise background at ~1.6 m wavelength in several MOC images of the NPLD [*Perron and Huybers*, 2009], as suggested by *Fishbaugh et al.* [2010b]. The consistent thickness of individual fine beds across several columns is suggestive of a quasiperiodic control on fine bed thickness for the NPLD. Whether the consistent thickness of fine beds is related to self-organization within the Mars climate system, or to external forcing on orbital or sub-orbital [*Weedon*, 2003] timescales, represents an important and unresolved question. Numerous terrestrial sedimentary environments show high-frequency cycles in stratigraphy that may result from intrinsic organization [*Einsele et al.*, 1991]. Alternatively, *Levrard et al.* [2007] suggest that several beds could form during one orbital cycle, particularly if ice and dust are sourced from multiple reservoirs. The meter-scale beds are considerably finer than those produced by the climate model

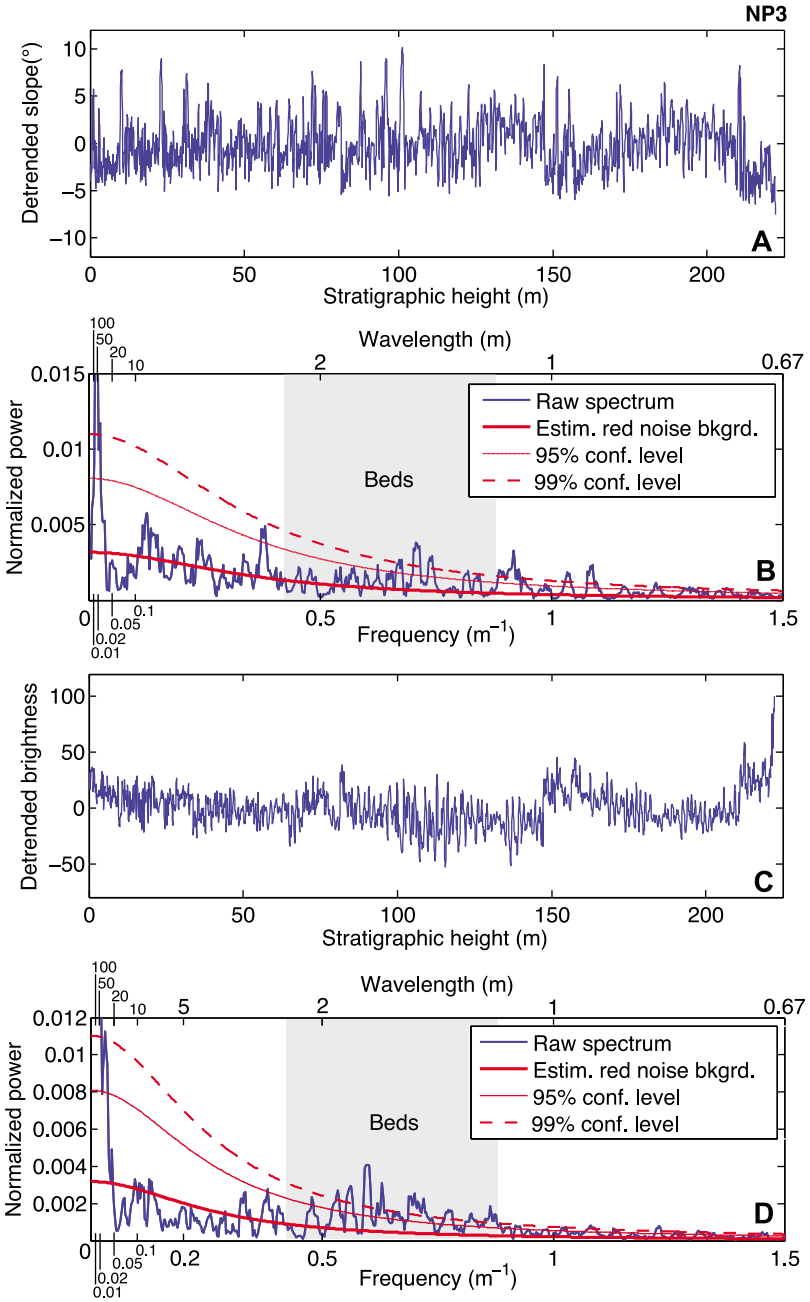

Figure 8. (a) Detrended image gray scale values for the stratigraphic transect at site NP3. (b) Power spectrum of data in Figure 8a. Shaded portion corresponds to 1-σ range of bed thickness measurements at same site. (c) Detrended slope, same location and reference frame as Figure 8a. (d) Power spectrum of data in Figure 8c. Shaded portion corresponds to 1-σ range of bed thickness measurements at the same site.

of *Levrard et al.* [2007], in which beds are emplaced in response to orbital cycles and range in thickness from 10 to 80 m. However, influences on bed characteristics from local topography, seasonal effects, dust cycles [*Levrard et al.*, 2007], and the distribution and evolution of shallow subsurface ice at lower latitudes [*Boynton et al.*, 2002; *Schorghofer*, 2007] remain to be considered in future models.

[38] SPLD bed thickness measurements show much greater variability than corresponding measurements for the NPLD (Figure 11), and the SPLD beds lack the morphologic and albedo differences that distinguish fine beds from marker beds in the NPLD. The large variance in bed thickness either argues against periodic forcing for generating the stratigraphy at the SPLD sites, or alternatively suggests that processes inherent to bed generation overwhelmed any orbital forcing of ice and dust cycles. The large difference in stratigraphic exposure age implied by surface exposure ages [*Herkenhoff and Plaut*, 2000; *Koutnik et al.*, 2002; *Tanaka et al.*, 2008] likely has some influence on exposed stratigraphy, and could render fine beds relatively more susceptible

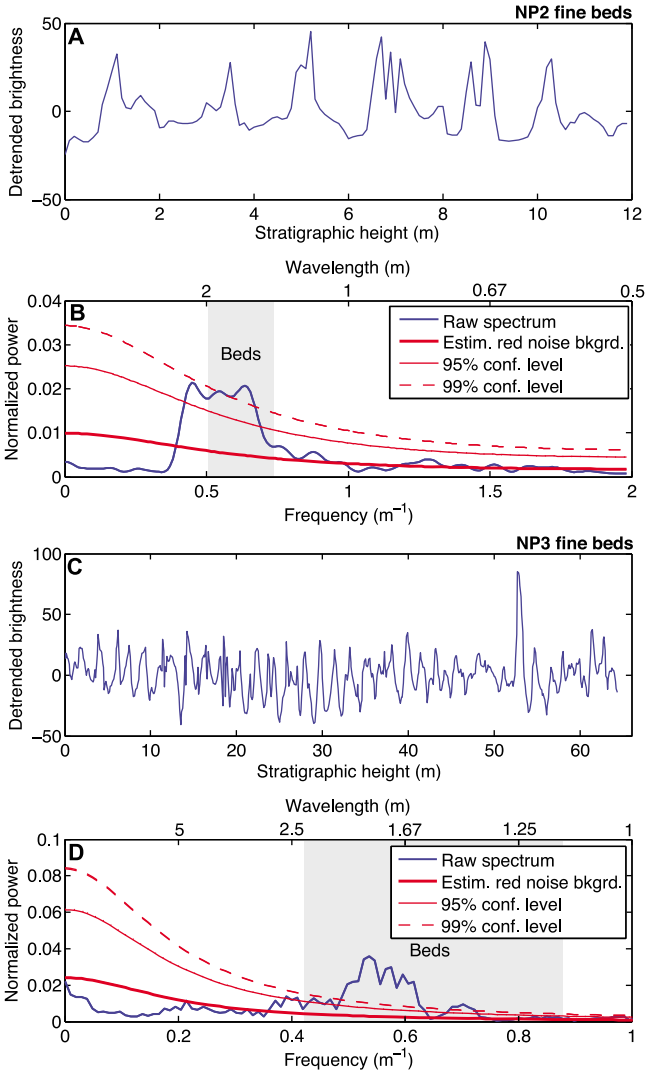

Figure 9. (a) Detrended image gray scale values for a section of fine beds at site NP2, in a stratigraphic reference frame corrected for topography and bed orientation. (b) Power spectrum of data in Figure 9a. Shaded portion corresponds to 1-σ range of bed thickness measurements at site NP2. (c) Detrended image gray scale values for a section of fine beds at site NP3, in stratigraphic reference frame. (d) Power spectrum of data in Figure 9c. Shaded portion corresponds to 1-σ range of bed thickness measurements at site NP3, including fine beds and marker beds.

to being obscured in the SPLD compared to the NPLD. However, partially obscured fine bed sets are uncommon in the measured SPLD sections, and the overall SPLD bed thickness distribution (Figure 11) does include beds as fine as 1.8 m. Therefore while we cannot rule out such processes, the observed stratigraphy does not obviously imply obscuring or amalgamation of fine beds.

[39] Additional sites within the SPLD may yet reveal a class of beds similar to the fine beds at sites NP1, NP2 and NP3; sites SP2 and SP3 are located close to the margin of the SPLD and represent basal exposures. However, no evidence is found to suggest a change in the character of stratigraphy with depth or geographic location within the SPLD comparable to the difference between the NPLD and the Planum Boreum Cavi [*Tanaka and Kolb*, 2001].

[40] Spectral analysis confirms the quasiperiodicity of fine beds in the NPLD. Several factors influence the brightness of the polar layered deposits, including roughness, outcrop-scale slope, and surficial modification [*Fishbaugh et al.*, 2010a]. It would be surprising if brightness were independent of bed properties, including ice grain size and dust fraction. The extrinsic influences on brightness may thus complement, rather than completely overprint, compositional signals recorded in the remotely observable stratigraphy. If repeating patterns in brightness do occur and can be linked to independent measurements of bed or unit thickness, as has been done in this study, then it seems likely that the signals in image brightness reveal bed properties. The brightness variations most likely reflect (1) slope variations dictated by the stratigraphy itself, or (2) intrinsic variations in bed albedo. Measurements of bed thickness, coupled with spectral analysis of brightness and slope, demonstrate that quasiperiodic bed sequences occur at multiple locations in the NPLD, and that in these areas brightness variations are unlikely to be an artifact of roughness, frost, or outcrop-scale slope. This suggests that fine bed sets within the PLDs are recording repeating events that have similar outcomes for the accumulation of ice and dust. In contrast, power spectra of slope and brightness show no consistent wavelength of stratigraphic organization at three SPLD sites, an observation that is also consistent with direct bed thickness measurements.

[41] With a data set expanded to include bed thickness measurements for three sites within the NPLD and three additional sites within the SPLD, the emerging picture indicates that the only discernable periodicity within the PLD is the consistency for fine bed thickness within the NPLD, a result consistent with previous analyses of the NPLD [*Perron and Huybers*, 2009] that is confirmed here with higher-resolution data. This interpretation is consistent with the

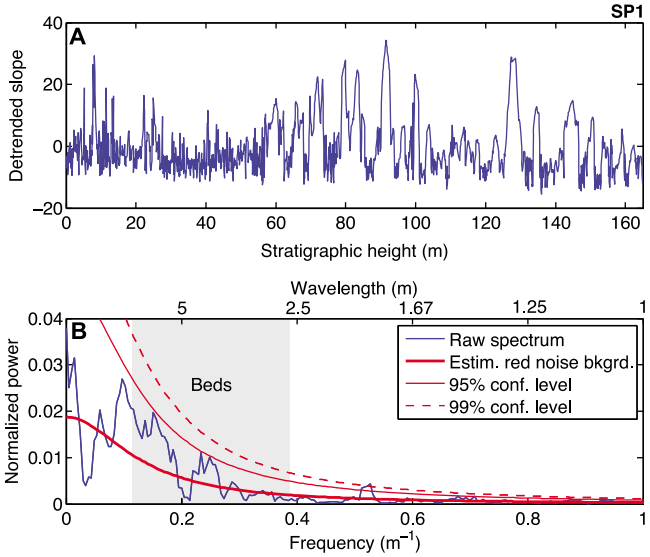

Figure 10. (a) Detrended slope for the stratigraphic transect at site SP1. (b) Power spectrum of data in Figure 10a. Shaded portion corresponds to 1-σ range of bed thickness measurements at same site.

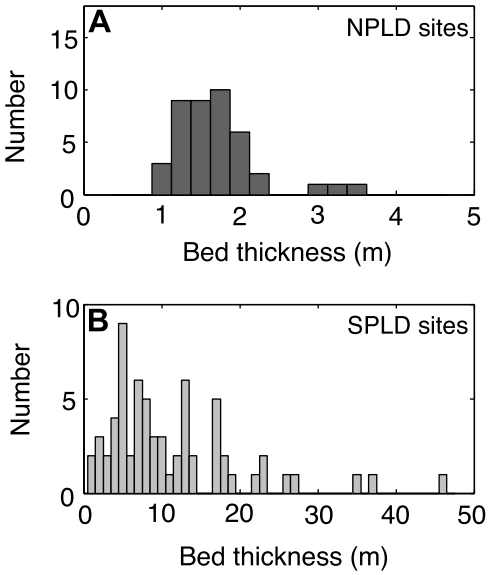

Figure 11. Summary of bed thickness measurements for sites within (a) the NPLD, binned at 0.25 m intervals, and (b) the SPLD, binned at 1 m intervals.

SPLD sites analyzed here, which contain no bed-controlled, quasiperiodic signals, but other SPLD sites imaged by HiRISE do occasionally possess adjacent beds which appear fine and of potentially similar thickness (e.g., images PSP_004707_0990 and ESP_014360_0985). These locations also include basal exposures of the SPLD, as at sites SP2 and SP3. Such locations warrant further investigation with high-resolution topographic data, as apparent bed thickness can be deceptive without detailed analysis to account for bed orientation and topographic exposure. If fine bed sequences are major components of the stratigraphy at other SPLD sites, this would suggest lateral variability in SPLD fine bed accumulation, as such sequences are not observed at the sites studied here. Such a result would contrast with the NPLD stratigraphy, in which thickness of individual stratigraphic horizons varies longitudinally [*Fishbaugh and Hvidberg*, 2006] but the facies types appear consistent across large distances; however, a spotty distribution of fine beds in the SPLD would be consistent with the finding that the large-scale stratigraphy of the SPLD reflects regional variation in net accumulation [*Milkovich and Plaut*, 2008]. If, as suggested by sites SP1-SP3, fine bed sequences are generally rare in the SPLD, it may represent a fundamental difference between the accumulation history of the NPLD and SPLD.

[42] Future observations extending beyond the spatial scale of this study may alter or lend support to this trend. PLD stratigraphy has been shown to correlate laterally within portions of the NPLD [*Fishbaugh and Hvidberg*, 2006], but not yet at the scale of fine bed sets [*Fishbaugh et al.*, 2010b]. Moreover, controls on the slope of PLD surfaces remain largely unexplored. Estimates from radar, gravity and topography data indicate a dustier bulk composition for the SPLD than for the NPLD. We speculate that the difference in bed prominence may owe in part to dust content. If so, the departure of trough topography from a stair-stepped profile could be used to constrain bed composition [*Byrne et al.*, 2011].

7. Conclusions

[43] This study presents two quantitative stratigraphic columns of the NPLD, the first three bed thickness profiles of the SPLD using HiRISE data, and refined spectral estimates of PLD brightness and slope using high-resolution digital elevation models. Observations at three sites—separated from each other by hundreds of kilometers—suggest consistent stratigraphic characteristics of the NPLD at 1 m horizontal resolution. Direct measurements of bed thickness show that beds 1–2 m thick are common all three NPLD sites. Marker beds, distinguished by their topographic prominence and low albedo, exhibit thicknesses with greater mean and comparable variance. Neither the thickness of fine bed sets nor the separation distance of marker beds within the NPLD has a characteristic value. Using the criteria of topographic prominence and albedo, the SPLD transects include only one type of bed, and the bed thickness shows greater mean and variance than observed for the NPLD fine beds. Data show little evidence for bed compaction at any site, nor waning bed thickness near unconformities. The consistent thickness of fine beds within the NPLD currently represents the only evidence for a quasi-periodic component of PLD stratigraphy.

[44] **Acknowledgments.** This work was supported by the van Wingen Fellowship, the W. M. Keck Institute for Space Studies, and the NASA Mars Data Analysis Program, award 65P-1089493. Kevin Lewis provided valuable consultation, and Terry-Ann Suer and Michael Lauria contributed to stereogrammetry processing. We gratefully acknowledge the HiRISE Team for the image data, and thank Sarah Milkovich and an anonymous reviewer for comments that greatly improved this manuscript.

References

Banks, M. E., S. Byrne, K. Galla, A. S. McEwen, V. J. Bray, C. M. Dundas, K. E. Fishbaugh, K. E. Herkenhoff, and B. C. Murray (2010), Crater population and resurfacing of the Martian north polar layered deposits, *J. Geophys. Res.*, *115*, E08006, doi:10.1029/2009JE003523.

Bibring, J. P., et al. (2004), Perennial water ice identified in the south polar cap of Mars, *Nature*, *428*, 627–630, doi:10.1038/nature02461.

Boynton, W. V., et al. (2002), Distribution of hydrogen in the near surface of Mars: Evidence for subsurface ice deposits, *Science*, *297*, 81–85, doi:10.1126/science.1073722.

Byrne, S. (2009), The polar deposits of Mars, *Annu. Rev. Earth Planet. Sci.*, *37*, 535–560, doi:10.1146/annurev.earth.031208.100101.

Byrne, S., and A. B. Ivanov (2004), Internal structure of the Martian south polar layered deposits, *J. Geophys. Res.*, *109*, E11001, doi:10.1029/2004JE002267.

Byrne, S., et al. (2011), Exposure analysis of polar stratigraphy from HiRISE topography, *LPI Contrib.*, *1323*, 6012.

Cutts, J. A., and B. H. Lewis (1982), Models of climatic cycles record in Martian polar layered deposits, *Icarus*, *50*, 216–244, doi:10.1016/0019-1035(82)90124-5.

Einsele, G., W. Ricken, and A. Seilacher (1991), Cycles and events in stratigraphy—Basic concepts and terms, in *Cycles and Events in Stratigraphy*, edited by G. Einsele, W. Ricken, and A. Seilacher, pp. 1–19, Springer, Berlin.

Fenton, L. K., and K. E. Herkenhoff (2000), Topography and stratigraphy of the northern Martian polar layered deposits using photoclinometry, stereogrammetry, and MOLA altimetry, *Icarus*, *147*, 433–443, doi:10.1006/icar.2000.6459.

Fishbaugh, K. E., and C. S. Hvidberg (2006), Martian north polar layered deposits stratigraphy: Implications for accumulation rates and flow, *J. Geophys. Res.*, *111*, E06012, doi:10.1029/2005JE002571.

Fishbaugh, K. E., S. Byrne, K. E. Herkenhoff, R. L. Kirk, C. Fortezzo, P. S. Russell, and A. McEwen (2010a), Evaluating the meaning of "layer" in the Martian north polar layered deposits and the impact on the climate connection, *Icarus*, *205*, 269–282, doi:10.1016/j.icarus.2009.04.011.

Fishbaugh, K. E., C. S. Hvidberg, S. Byrne, P. S. Russell, K. E. Herkenhoff, M. Winstrup, and R. Kirk (2010b), First high-resolution stratigraphic column of the Martian north polar layered deposits, *Geophys. Res. Lett.*, *37*, L07201, doi:10.1029/2009GL041642.

Forget, F., R. M. Haberle, F. Montmessin, B. Levrard, and J. W. Head (2006), Formation of glaciers on Mars by atmospheric precipitation at high obliquity, *Science*, *311*, 368–371, doi:10.1126/science.1120335.

Hays, J. D., J. Imbrie, and N. J. Shackleton (1976), Variation in the earth's orbit: Pacemaker of the ice ages, *Science*, *194*, 1121–1132, doi:10.1126/science.194.4270.1121.

Head, J. W., J. F. Mustard, M. A. Kreslavsky, R. E. Milliken, and D. R. Marchant (2003), Recent ice ages on Mars, *Nature*, *426*, 797–802, doi:10.1038/nature02114.

Head, J. W., et al. (2005), Tropical to mid-latitude snow and ice accumulation, flow and glaciation on Mars, *Nature*, *434*, 346–351, doi:10.1038/nature03359.

Herkenhoff, K. E., and R. L. Kirk (2001), MOC Photoclinometry of the Polar Layered Deposits on Mars, *Lunar Planet. Sci.*, *XXXII*, Abstract 1129.

Herkenhoff, K. E., and J. J. Plaut (2000), Surface ages and resurfacing rates of the polar layered deposits on Mars, *Icarus*, *144*, 243–253, doi:10.1006/icar.1999.6287.

Herkenhoff, K. E., S. Byrne, P. S. Russell, K. E. Fishbaugh, and A. S. McEwen (2007), Meter- scale morphology of the north polar region of Mars, *Science*, *317*, 1711–1715, doi:10.1126/science.1143544.

Hess, S. L., J. A. Ryan, J. E. Tillman, R. M. Henry, and C. B. Leovy (1980), The annual cycle of pressure on Mars measured by Viking landers 1 and 2, *Geophys. Res. Lett.*, *7*, 197–200, doi:10.1029/GL007i003p00197.

Howard, A. D., J. A. Cutts, and K. R. Blasius (1982), Stratigraphic relationships within Martian polar cap deposits, *Icarus*, *50*, 161–215, doi:10.1016/0019-1035(82)90123-3.

Jakosky, B. M., B. G. Henderson, and M. T. Mellon (1993), The Mars water cycle at other epochs: Recent history of the polar caps and layered terrains, *Icarus*, *102*, 286–297, doi:10.1006/icar.1993.1049.

Jakosky, B. M., B. G. Henderson, and M. T. Mellon (1995), Chaotic obliquity and the nature of the Martian climate, *J. Geophys. Res.*, *100*, 1579–1584, doi:10.1029/94JE02801.

Kirk, R. L., et al. (2008), Ultrahigh resolution topographic mapping of Mars with MRO HiRISE stereo images: Meter-scale slopes of candidate Phoenix landing sides, *J. Geophys. Res.*, *113*, E00A24, doi:10.1029/2007JE003000.

Kolb, E. J., and K. L. Tanaka (2001), Geological history of the polar regions of Mars based on Mars Global Surveyor data, II, Amazonian period, *Icarus*, *154*, 22–39, doi:10.1006/icar.2001.6676.

Kolb, E. J., and K. L. Tanaka (2006), Accumulation and erosion of south polar layered deposits in the Promethei Lingula region, Planum Australe, Mars, *Mars*, *2*, 1–9, doi:10.1555/mars.2006.0001.

Koutnik, M., S. Byrne, and B. Murray (2002), South polar layered deposits of Mars: The cratering record, *J. Geophys. Res.*, *107*(E11), 5100, doi:10.1029/2001JE001805.

Langevin, Y., F. Poulet, J. P. Bibring, B. Schmitt, S. Douté, and B. Gondet (2005), Summer evolution of the north polar cap of Mars as observed by OMEGA/Mars Express, *Science*, *307*, 1581–1584, doi:10.1126/science.1109438.

Laskar, J., B. Levrard, and J. F. Mustard (2002), Orbital forcing of the Martian polar layered deposits, *Nature*, *419*, 375–377, doi:10.1038/nature01066.

Laskar, J., A. C. M. Correia, M. Gastineau, F. Joutel, B. Levrard, and P. Robutel (2004), Long term evolution and chaotic diffusion of the insolation quantities of Mars, *Icarus*, *170*, 343–364, doi:10.1016/j.icarus.2004.04.005.

Levrard, B., F. Forget, F. Montmessin, and J. Laskar (2007), Recent formation and evolution of northern Martian polar layered deposits as inferred from a global climate model, *J. Geophys. Res.*, *112*, E06012, doi:10.1029/2006JE002772.

Lewis, K. W., O. Aharonson, J. P. Grotzinger, R. L. Kirk, A. S. McEwen, and T. A. Suer (2008), Quasi-periodic bedding in the sedimentary rock record of Mars, *Science*, *322*, 1532–1535, doi:10.1126/science.1161870.

Lilliefors, H. W. (1967), On the Kolmogorov-Smirnov test for normality with mean and variance unknown, *J. Am. Stat. Assoc.*, *62*, 399–402.

Malin, M. C., and K. S. Edgett (2001), Mars Global Surveyor Mars Orbiter Camera: Interplanetary cruise through primary mission, *J. Geophys. Res.*, *106*, 23,429–23,570, doi:10.1029/2000JE001455.

Mann, M. E., and J. M. Lees (1996), Robust estimation of background noise and signal detection in climatic time series, *Clim. Change*, *33*, 409–445, doi:10.1007/BF00142586.

McEwen, A. S., et al. (2007), Mars Reconnaissance Orbiter's High Resolution Imaging Science Experiment (HiRISE), *J. Geophys. Res.*, *112*, E05S02, doi:10.1029/2005JE002605.

Mellon, M. T. (1996), Limits on the CO_2 content of the Martian polar deposits, *Icarus*, *124*, 268–279, doi:10.1006/icar.1996.0203.

Milkovich, S. M., and J. W. Head (2005), North polar cap of Mars: Polar layered deposit characterization and identification of a fundamental climate signal, *J. Geophys. Res.*, *110*, E01005, doi:10.1029/2004JE002349.

Milkovich, S. M., and J. J. Plaut (2008), Martian south polar layered deposit stratigraphy and implications for accumulation J history, *J. Geophys. Res.*, *113*, E06007, doi:10.1029/2007JE002987.

Milkovich, S. M., J. W. Head, G. Neukum, and the HRSC Team (2008), Stratigraphic analysis of the northern polar layered deposits of Mars: Implications for recent climate history, *Planet. Space Sci.*, *56*, 266–288, doi:10.1016/j.pss.2007.08.004.

Milkovich, S. M., J. J. Plaut, A. Safaeinili, G. Picardi, R. Seu, and R. J. Phillips (2009), Stratigraphy of Promethei Lingula, south polar layered deposits, Mars, in radar and imaging data sets, *J. Geophys. Res.*, *114*, E03002, doi:10.1029/2008JE003162.

Murray, B. C., W. R. Ward, and S. C. Yeung (1973), Periodic insolation variations on Mars, *Science*, *180*, 638–640, doi:10.1126/science.180.4086.638.

Murray, B. M., M. Koutnik, S. Byrne, L. Soderblom, K. Herkenhoff, and K. L. Tanaka (2001), Preliminary geological assessment of the northern edge of Ultimi Lobe, Mars south polar layered deposits, *Icarus*, *154*, 80–97, doi:10.1006/icar.2001.6657.

Nye, J. F., W. B. Durham, P. M. Schenk, and J. M. Moore (2000), The instability of a south polar cap on Mars composed of carbon dioxide, *Icarus*, *144*, 449–455, doi:10.1006/icar.1999.6306.

Okubo, C. (2010), Structural geology of Amazonian-aged layered sedimentary deposits in southwest Candor Chasma, Mars, *Icarus*, *207*, 210–225, doi:10.1016/j.icarus.2009.11.012.

Pathare, A. V., D. A. Paige, and E. Turtle (2005), Viscous relaxation of craters within the Martian south polar layered deposits, *Icarus*, *174*, 396–418, doi:10.1016/j.icarus.2004.10.031.

Perron, J. T., and P. Huybers (2009), Is there an orbital signal in the polar layered deposits on Mars?, *Geology*, *37*(2), 155–158, doi:10.1130/G25143A.1.

Phillips, R. J., et al. (2008), Mars north polar deposits: Stratigraphy, age, and geodynamical response, *Science*, *320*, 1182–1185, doi:10.1126/science.1157546.

Phillips, R. J., et al. (2011), Massive CO_2 ice deposits sequestered in the south polar layered deposits of Mars, *Science*, *332*, 838–841, doi:10.1126/science.1203091.

Picardi, G., J. J. Plaut, D. Biccari, O. Bombaci, and D. Calabrese (2005), Radar soundings of the subsurface of Mars, *Science*, *310*, 1925–1928, doi:10.1126/science.1122165.

Piqueux, S., C. S. Edwards, and P. R. Christensen (2008), Distribution of the ices exposed near the south pole of Mars using Thermal Emission Imaging System (THEMIS) temperature measurements, *J. Geophys. Res.*, *113*, E08014, doi:10.1029/2007JE003055.

Plaut, J. J., et al. (2007), Subsurface radar sounding of the south polar layered deposits of Mars, *Science*, *316*, 92–95, doi:10.1126/science.1139672.

Schorghofer, N. (2007), Dynamics of ice ages on Mars, *Nature*, *449*, 192–194, doi:10.1038/nature06082.

Sori, M., T. Perron, P. Huybers, and O. Aharonson (2011), Preservation of orbital signals in the Martian polar layered deposits, *LPI Contrib.*, *1323*, 6063.

Tanaka, K. L. (2005), Geology and insolation-driven climatic history of Amazonian north polar materials on Mars, *Nature*, *437*, 991–994, doi:10.1038/nature04065.

Tanaka, K. L., and E. J. Kolb (2001), Geologic history of the polar regions of Mars based on Mars Global Surveyor data, *Icarus*, *154*, 3–21, doi:10.1006/icar.2001.6675.

Tanaka, K. L., and E. J. Kolb (2005), Geologic mapping of the polar regions of Mars: Preliminary results and climate implications, *U.S. Geol. Surv. Open File Rep.*, *2005–1271*, 47–48.

Tanaka, K. L., and D. H. Scott (1987), Geologic map of the polar regions of Mars, *U.S. Geol. Surv. Misc. Invest. Ser. Map*, *I-1802-BC*.

Tanaka, K. L., A. P. Rodriguez, J. A. Skinner, M. C. Bourke, C. M. Fortezzo, K. E. Herkenhoff, E. L. Kolb, and C. H. Okubo (2008), North polar region of Mars: Advances in stratigraphy, structure, and erosional modification, *Icarus*, *196*, 318–358, doi:10.1016/j.icarus.2008.01.021.

Thomas, P., S. Squyres, K. Herkenhoff, A. Howard, and B. Murray (1992), Polar deposits of Mars, in *Mars*, edited by H. H. Kieffer et al., pp. 767–795, Univ. of Ariz. Press, Tucson.

Thomson, D. J. (1982), Spectrum estimation and harmonic analysis, *IEEE Proc.*, *70*, 1055–1096, doi:10.1109/PROC.1982.12433.

Toon, O. B., J. B. Pollack, W. Ward, J. A. Burns, and K. Bilski (1980), The astronomical theory of climatic change on Mars, *Icarus*, *44*, 552–607, doi:10.1016/0019-1035(80)90130-X.

Ward, W. R. (1973), Large-scale variations in the obliquity of Mars, *Science*, *181*, 260–262, doi:10.1126/science.181.4096.260.
Weedon, G. P. (2003), *Time-Series Analysis and Cyclostratigraphy*, Cambridge Univ. Press, New York, doi:10.1017/CBO9780511535482.
Wieczorek, M. A. (2008), Constraints on the composition of the Martian south polar cap from gravity and topography, *Icarus*, *196*, 506–517, doi:10.1016/j.icarus.2007.10.026.
Zuber, M. T., R. J. Phillips, J. C. Andrews-Hanna, S. W. Asmar, A. S. Konopliv, F. G. Lemoine, J. J. Plaut, D. E. Smith, and S. E. Smrekar (2007), Density of Mars' south polar layered deposits, *Science*, *317*(5845), 1718–1719, doi:10.1126/science.1146995.